Bioorganic & Medicinal Chemistry 21 (2013) 1006–1017

Contents lists available at SciVerse ScienceDirect

Bioorganic & Medicinal Chemistry

journal homepage: www.elsevier.com/locate/bmc

Design, synthesis, and evaluation of a water-soluble antofine analogue with high antiproliferative and antitumor activity

Yongseok Kwon [a,†], Jayoung Song [a,†], Boeun Lee [a], Jinkyung In [a], Hohyun Song [b], Hwa-Jin Chung [a], Sang Kook Lee [a,*], Sanghee Kim [a,*]

[a] College of Pharmacy, Seoul National University, San 56-1, Shilim, Kwanak, Seoul 151-742, Republic of Korea
[b] College of Pharmacy, Ewha Womans University, 11-1, Daehyun-dong, Seodaemun-gu, Seoul 120-750, Republic of Korea

ARTICLE INFO

Article history:
Received 28 September 2012
Revised 12 November 2012
Accepted 16 November 2012
Available online 4 December 2012

Keywords:
Antitumor activity
Antofine
Hydrophilic analogue
Multidrug resistance
Phenanthroindolizidine

ABSTRACT

New water soluble antofine C-13a analogues were designed, synthesized, and evaluated for antiproliferative activity against cancer cells. Particularly, (−)-(*R*)-13a-hydroxymethylantofine ((−)-(*R*)-**4b**) demonstrated notable growth inhibition against a panel of human cancer cell lines. This growth inhibition was associated with the arrest of the cell cycle in the G0/G1 phases and suppression of mTOR signaling in human lung A549 cancer cells. Compound (−)-(*R*)-**4b** also overcame paclitaxel-resistance in human lung cancer cells (A549-Pa) by suppressing P-glycoprotein expression. Furthermore, compound (−)-(*R*)-**4b** significantly inhibited the tumor growth of A549 and A549-Pa xenografts in a nude mouse model, which suggests it is a promising novel antitumor agent with sufficient aqueous solubility.

1. Introduction

Phenanthroindolizidine alkaloids are a small group of pentacyclic natural products primarily isolated from *Cynanchum*, *Pergularia*, *Tylophora*, and some genera of the Asclepiadaceae family.[1,2] (−)-Antofine (**1**, Fig. 1), (−)-tylophorine (**2**), and tylocrebrine (**3**) are representative phenanthroindolizidine alkaloids. The most intriguing biological property of this class of natural products is its profound cytotoxic activity against various cancer cell lines, including multidrug-resistant cell lines. For instance, (−)-antofine has IC_{50} values in the low nanomolar range against both multidrug-resistant KB-V1 and drug-sensitive KB-3-1 cancer cell lines, which is comparable to that of clinically used cytotoxic agents.[3,4] Although the biological targets are currently unclear, phenanthroindolizidine alkaloids have received significant attention as potential therapeutic agents because of their cytotoxicity and unique mode of action.[5] However, this class of natural products has not yet been developed for clinical use due to several pharmacologically unsuitable properties. Therefore, intense medicinal chemical investigations have been conducted[5–7] and indicate that further structural modifications are necessary.

The primary drawbacks to the therapeutic use of phenanthroindolizidine alkaloids are their central nervous system (CNS) toxicity[8,9] and low water solubility. As polar substances have lower tendencies to cross the blood–brain barrier (BBB), it was proposed that the CNS side effects of phenanthroindolizidine alkaloids could be minimized by introducing hydrophilic groups.[8] The aqueous solubility of small molecules also generally increases with increasing hydrophilicity. Therefore, enhancing their hydrophilicity via chemical modification might be a reasonable strategy for improving the pharmacological properties of phenanthroindolizidine alkaloids. However, only a few types of polar analogues have been synthesized and evaluated.[7] One such type is the antofine derivatives **5a–c** (Fig. 1), which incorporate an N or O atom into the E-ring.[7b] Another notable type is tylophorine derivatives **6a–b**, which have a hydroxyl group at C-14.[7f] Although most polar analogues were generally appreciably less potent, some exhibited comparable in vitro cytotoxicities to those observed for the parent phenanthroindolizidine alkaloids.

The structure–activity relationship (SAR), which is obtained by comparing the cytotoxic activities of the various natural phenanthroindolizidine alkaloids and their synthetic analogues, indicates that the cytotoxic potency is highly sensitive to the type and pattern of substitutions on the phenanthrene ring.[3,7c,f,g] Furthermore, it has been concluded that rigid phenanthrene and indolizidine rings are required to maintain potent cytotoxic activities.[3,7e,h] In other words, the pentacyclic ring system of the phenanthroindolizidine structure is essential for a high cytotoxic activity.

* Corresponding authors. Tel.: 82 2 880 2475; fax: 82 2 762 8322 (S.K.L.); tel.: 82 2 880 2487; fax: 82 2 888 0649 (S.K.).
E-mail addresses: sklee61@snu.ac.kr (S.K. Lee), pennkim@snu.ac.kr (S. Kim).
† These two authors contributed equally to this work.

0968-0896/$ - see front matter © 2012 Elsevier Ltd. All rights reserved.
http://dx.doi.org/10.1016/j.bmc.2012.11.039

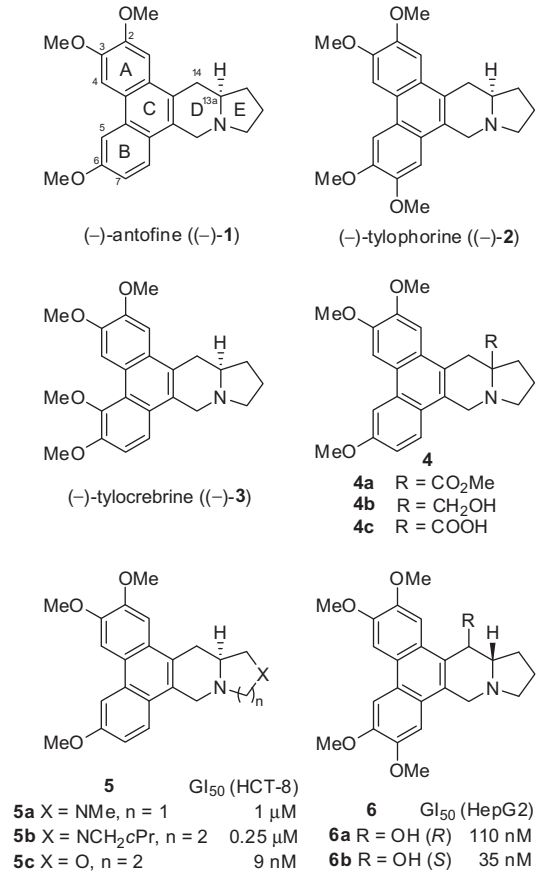

Figure 1. Chemical structures of compounds **1**–**6**.

In an attempt to reduce the drawbacks of phenanthroindolizidine alkaloids while retaining both the essential pentacyclic core and typical substitution patterns of the phenanthrene ring, we designed compounds with the general structure of **4** (Fig. 1), where the hydrogen atom at C-13a in antofine was replaced with a hydrophilic group such as hydroxylmethyl or carboxylic acid. In this study, we employed antofine as a model phenanthroindolizidine alkaloid because of its very high potency and well-established SAR studies.[3,5,7g] We envisioned that this modification would increase the hydrophilic character of the molecule, thus lowering the BBB permeability and increasing the water solubility.[10] In addition, the substituent at C-13a would disrupt the molecular planarity, which decreases the crystal packing energy and consequently increases the solubility.[11] Our theoretical calculations indicated that, as expected, the relatively more polar **4a**, **4b**, and **4c** were predicted to have better log BB values of −0.15, −0.06, and −0.38, respectively, compared to 0.33 for antofine.[12] The calculated water solubility of **4a**, **4b**, and **4c** were 0.208, 0.916, and 0.491 μg/mL, respectively, while that of antofine was only 0.088 μg/mL.[13]

We herein report both the efficient synthesis of the designed water-soluble antofine analogues[14] and the evaluation of their growth inhibitory activity and mechanism of action against cancer cells. The antitumor activity of in vivo xenograft models for the active compound (−)-(*R*)-**4b** was also demonstrated.

2. Results and discussion

2.1. Design, synthesis and growth inhibition of cancer cells

The designed C-13a substituted antofine analogues, **4a**–**c**, were synthesized in their racemic forms as shown in Scheme 1. Commercially available *N*-Boc-L-proline methyl ester was alkylated

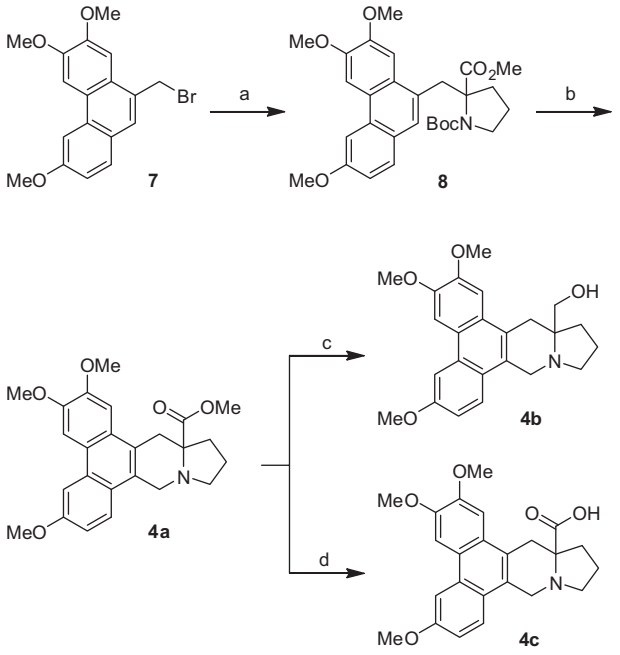

Scheme 1. Synthesis of antofine C-13a analogues. Reagents and conditions: (a) *N*-Boc-L-ProOMe, LDA, HMPA, THF, −78 °C; (b) HCHO, *c*-HCl, EtOH, reflux; (c) $LiAlH_4$, THF, 0 °C; (d) LiOH, THF, reflux.

with the known phenanthryl bromide **7**[15] to afford racemic **8** in 71% yield.[16] The obtained substance was directly subjected to the Pictet–Spengler conditions to achieve a one-pot pentacyclic core formation via *N*-Boc deprotection, iminium ion formation, and electrophilic aromatic substitution. When **8** was treated with formaldehyde and hydrochloric acid in refluxing EtOH, the desired pentacyclic product **4a** was obtained in 85% yield. The ester group in **4a** was either reduced with $LiAlH_4$ to yield the alcohol **4b** (88%) or hydrolyzed with LiOH to yield the carboxylic acid **4c** (81%).

The antiproliferative activities of the C-13a substituted antofine analogues **4a**–**c** were determined using a sulforhodamine B (SRB) assay for a preliminary evaluation.[4,17] As shown in Table 1, the ester analogue **4a** and acid analogue **4c** did not show any notable growth inhibition at the highest tested concentration of 1 μM. Although less potent than (±)-antofine, the hydroxymethyl analogue **4b** exhibited notable antiproliferative activity with IC_{50} values in the submicromolar range against the tested cancer cell lines. The only structural difference between the acid **4c** and the alcohol **4b** was the presence of a carbonyl group. This simple functional group difference significantly influenced the biological activity.

The thermodynamic aqueous solubilities of antofine (**1**) and its hydroxymethyl analogue **4b** were determined according to Avdeef and Testa.[18] The aqueous solubility of antofine in phosphate buffer (pH 7.4) was very low (<1 μg/mL). However, the hydroxymethyl analogue **4b** showed much better solubility (656 μg/mL) as expected based on our calculations. In a 1:1 mixture of phosphate buffer and EtOH, the solubility of **1** remained poor (47 μg/mL) while that of **4b** was very high (1392 μg/mL); indeed, analogue **4b** was 300 times more soluble than the parent compound **1**.

After identifying the racemic hydroxymethyl analogue **4b** as being notably antiproliferative and water soluble, both its (*R*)- and (*S*)-enantiomers were prepared to examine the growth-inhibitory effects of the chiral center at C-13a. Seebach's self-reproduction of chirality methodology[19] was used to introduce chirality at C-13a. The 2-alkylproline derivative (*R*,*R*)-**10** was synthesized in 71% yield from phenanthryl bromide **7** and oxazolidinone (3*R*,7a*S*)-**9** using Wang and Germanas's modification[20] to Seebach's method (scheme 2). The crude NMR spectrum showed that the reaction only

Table 1
Structure and antiproliferative activities for antofine ((±)-**1**) and its analogues ((±)-**4a–c**)

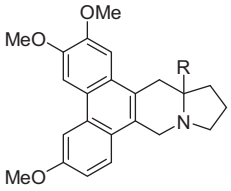

Compd	R	IC_{50}[a] (nM)					
		SK-HEP-1[b]	SNU638[c]	HCT15[d]	HCT116[d]	A549[e]	A549-Pa[f]
4a	$-CO_2Me$	>1 μM	>1 μM	>1 μM	>1 μM	>1 μM	>1 μM
4b	$-CH_2OH$	100 ± 12	92 ± 10	179 ± 9	53 ± 6	167 ± 13	204 ± 22
4c	–COOH	>1 μM	>1 μM	>1 μM	>1 μM	>1 μM	>1 μM
(±)-Antofine	–H	16 ± 2	21 ± 6	25 ± 6	11 ± 2	20 ± 5	22 ± 5

[a] All values are means of at least three experiments.
[b] Human liver cancer cells.
[c] Human stomach cancer cells.
[d] Human colorectal cancer cells.
[e] Human lung cancer cells.
[f] Paclitaxel-resistant human lung cancer cells (IC_{50} of paclitaxel = 321.2 nM for A549-Pa and 1.4 nM for A549).

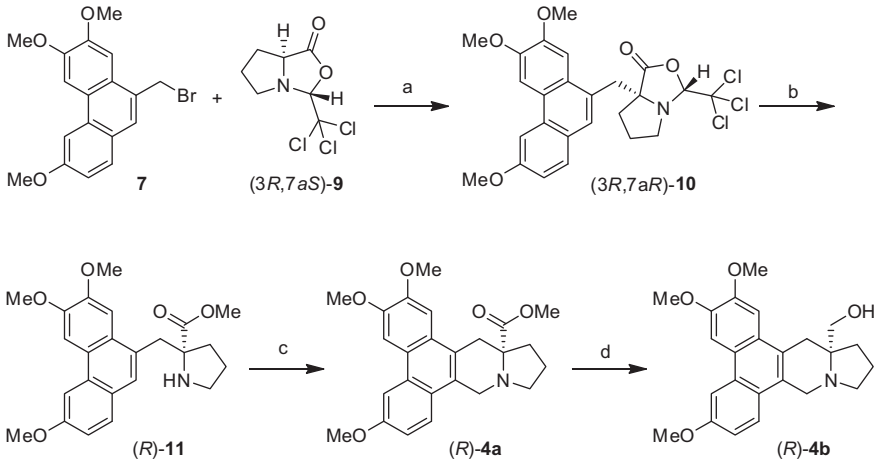

Scheme 2. Enantioselective synthesis of antofine C-13a analogues. Reagents and conditions: (a) LDA, THF, −78 °C; (b) AcCl, MeOH, reflux; (c) HCHO, *c*-HCl, EtOH, reflux; (d) $LiAlH_4$, THF, 0 °C.

produced a single diastereomer. The obtained proline oxazolidinone (*R*,*R*)-**10** was converted directly to the methyl ester (*R*)-**11** in 72% yield by refluxing in acidic anhydrous methanol. The Pictet–Spengler cyclomethylenation of (*R*)-**11** afforded (*R*)-**4a** in 80% yield. The ester group in (*R*)-**4a** was reduced with $LiAlH_4$ to produce (*R*)-**4b** in 91% yield. The (*S*)-isomeric form of **4b** was prepared from (3*S*,7a*R*)-**7** as described above.

The growth-inhibitory activities of both **4b** enantiomers were determined for various cancer cells. The naturally occurring enantiomeric form of antofine (−)-**1** was also tested for direct comparison. Table 2 shows that the (*S*)-isomeric form of **4b** has IC_{50} values in the low micromolar range against the tested cancer cell lines. However, its potency was significantly less than its (*R*)-isomeric form. This result indicated that the growth inhibition of the racemic **4b** is largely due to the (*R*)-enantiomer. The (*R*)-form of **4b** exhibited high antiproliferative activity against various types of human cancer cell lines. However, it was less potent than parent natural product (−)-**1** by approximately ten-fold.

These preliminary biological results revealed that the introduction of a hydrophilic substituent at C-13a decreased the activity. However, the antiproliferative activity of (*R*)-**4b** is still very high and comparable to that of conventional antitumor chemotherapeutic agents. This high potency and substantially improved aqueous solubility of (*R*)-**4b** prompted us to further investigate its biological properties and anticancer potential.

2.2. Compound (*R*)-4b induces G0/G1 cell cycle arrest

Based on the notable antiproliferative activity of (*R*)-**4b** for several cancer cells including drug-resistant cancer cells, further studies were conducted to determine the molecular mechanism of action in the inhibition of human lung cancer cell growth. Since lung cancer is the most common form of this disease in the world and the leading cause of cancer-associated human death,[21] the mechanistic investigation of cell proliferation by (*R*)-**4b** was performed using the A549 cell-line, which is sensitive to (*R*)-**4b** and is one of the most widely used human cancer cell lines.[22] Primarily, the cell cycle progression was evaluated using flow cytometry after treating human lung cancer A549 cells with (*R*)-**4b** for 24 h. As shown in Figure 2A, (*R*)-**4b** induced cell cycle arrest in the G0/G1

Table 2
Structure and antiproliferative activities for enantiomers of **4b**

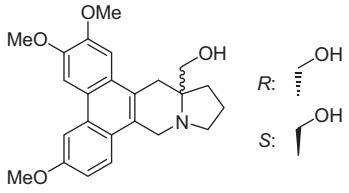

Compd.	IC_{50}[a] (nM)					
	SK-HEP-1[b]	SNU638[c]	HCT15[d]	HCT116[d]	A549[e]	A549-Pa[f]
(*R*)-**4b**	60 ± 9	80 ± 4	160 ± 7	60 ± 4	120 ± 13	200 ± 15
(*S*)-**4b**	540 ± 35	1490 ± 40	1420 ± 50	800 ± 34	2270 ± 80	3660 ± 92
(−)-Antofine	8 ± 3	10 ± 1	13 ± 2	8 ± 3	11 ± 1	18 ± 5

[a] All values are means of at least three experiments.
[b] Human liver cancer cells.
[c] Human stomach cancer cells.
[d] Human colorectal cancer cells.
[e] Human lung cancer cells.
[f] Paclitaxel-resistant human lung cancer cells (IC_{50} of paclitaxel = 321.2 nM for A549-Pa and 1.4 nM for A549).

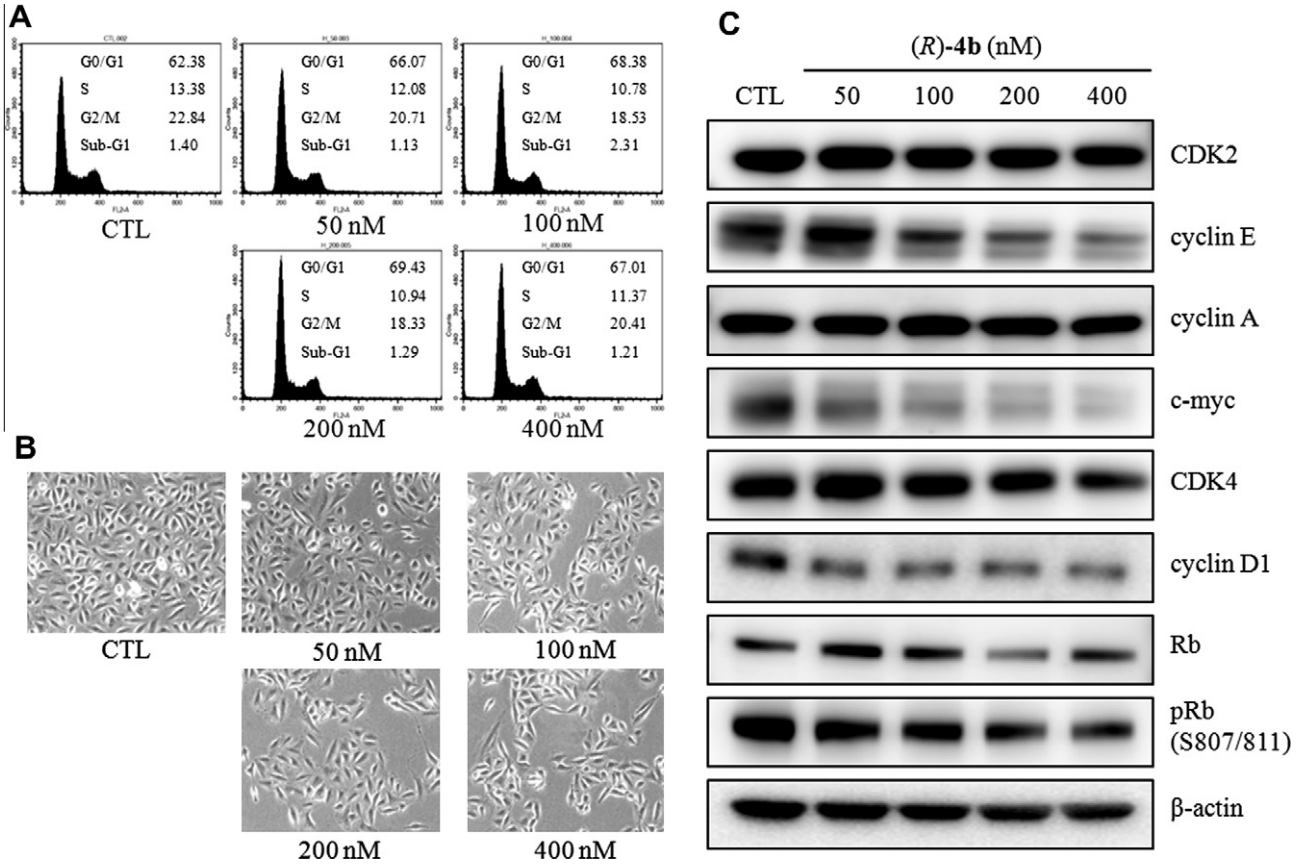

Figure 2. Effect of (*R*)-**4b** on cell cycle distribution in A549 cells. (**A**) A549 cells were incubated with (*R*)-**4b** for 24 h. After incubation, cells were fixed with 100% methanol and stained for 30 min with PBS containing propidium iodide (50 μg/mL) and RNase A (50 μg/mL) at room temperature. The cellular DNA content was analyzed by flow cytometry. (**B**) A549 cells were incubated with (*R*)-**4b** for 24 h. Cellular morphological changes were observed using an inverted phase-contrast microscope and photographed. (**C**) A549 cells were incubated with various concentrations of (*R*)-**4b** for 24 h, and the expression of cell cycle regulatory proteins was then analyzed by Western blot analysis.

phase; however, the distribution of the sub-G1 phase was not notably changed, which indicates apoptotic cell death did not contribute significantly to the inhibition of human lung cancer cell growth by (*R*)-**4b**. This finding was also consistent with the morphological changes discovered under an inverted phase-contrast microscope. As shown in Figure 2B, even though treatment with (*R*)-**4b** markedly decreased the number of cells, most cells were attached with barely any floating cells detected. When the

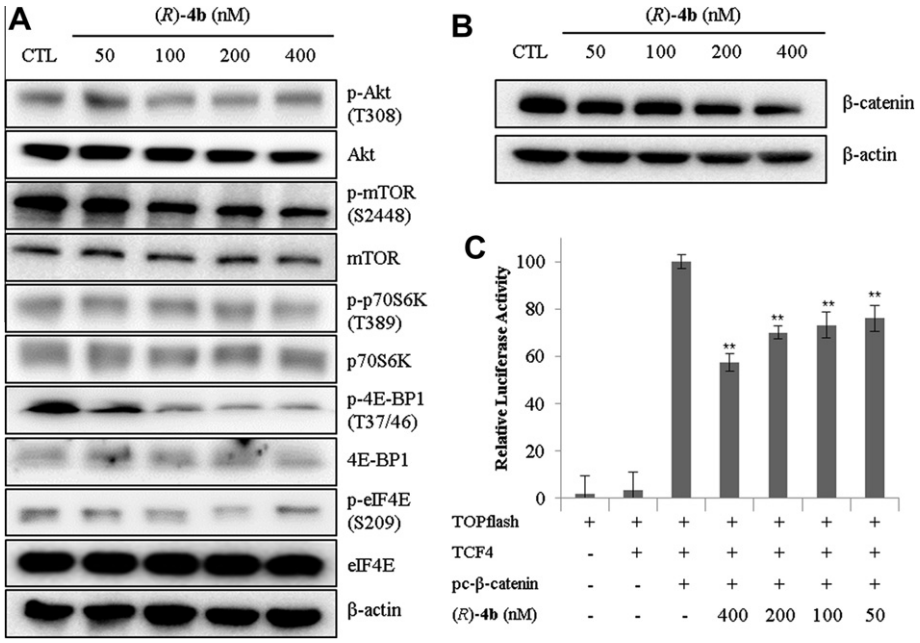

Figure 3. Modulation of Akt/mTOR and Wnt signaling by (*R*)-**4b**. A549 cells were treated with various concentrations of (*R*)-**4b** for 24 h, and then protein expressions for Akt/mTOR (**A**) and Wnt signaling (**B**) were analyzed by Western blot analysis. (**C**) HEK293 cells were transfected with TOPflash (β-catenin/Tcf reporter plasmids) and pRL-SV40 reporter plasmids for 24 h. After transfection, cells were incubated with (*R*)-**4b** for 24 h. Luciferase activity was measured by dual-luciferase reporter gene assay system. $^{**}p$ <0.01, compared with the DMSO control.

checkpoint protein expression associated with G0/G1 phase arrest was examined by Western blot analysis, the suppression of cyclin D1, cyclin E, CDK4, phospho-Rb, and c-myc was discovered; however, the expression of CDK2 was not significantly affected by treatment with (*R*)-**4b** (Fig. 2C).

2.3. Compound (*R*)-4b suppresses Akt/mTOR signaling pathways

To further investigate the molecular mechanism of (*R*)-**4b**, we analyzed the regulation of the cellular signal transduction pathway in the antiproliferative activity of the A549 cells. A body of evidence suggests that the proteins in the Akt/mTOR signaling pathway are upregulated and plays an important role in the growth and survival of human lung cancer cells. Akt is also associated with the positive regulation of the G0/G1 cell cycle progression via the modulation of Akt substrates such as c-myc. When treated with (*R*)-**4b**, the suppression of the activation of Akt was found as shown in Figure 3A, which indicated the inhibition of Akt/c-myc signaling by (*R*)-**4b** suppressed cyclins/CDK4 and Rb expression. These effects might arrest the cell cycle progression in the G0/G1 phase. In addition, mTOR, a downstream effector of the Akt signaling pathway, is also considered a pivotal modulator of cell proliferation in lung cancer cells. mTOR is activated by Akt upon its phosphorylation at Ser2448. The translational initiation of several survival proteins was also activated via mTOR signaling through the activation of the eukaryotic initiation factors 4E(eIF4E)-binding protein 1 (4EBP1) and eIF4E.[23] Therefore, the modulation of mTOR signaling is targeted a promising therapy for lung cancer. As shown in Figure 3A, (*R*)-**4b** suppressed the phosphorylation of mTOR and its downstream effectors such as 4E-BP1 and eIF4E. These findings demonstrate that (*R*)-**4b** inhibits the growth of A549 cells via the suppression of the constitutively activated Akt/mTOR signaling pathway.

2.4. Compound (*R*)-4b suppresses β-catenin-mediated transcriptional activity

We next analyzed the involvement of Wnt signaling in the antiproliferative activity of the A549 cells. Because (*R*)-**4b** suppressed cyclin D1 expression in A549 cells, the effect of (*R*)-**4b** on the activation of the Wnt signaling pathways, an upstream signaling regulating cyclin D1 expression, was examined. In general, the dysregulation of the Wnt signaling pathway is also known to be closely associated with human lung cancers. In the absence of Wnt, β-catenin is normally sequestered in cytoplasm via a destruction complex consisting of adenomatous polyposis coil (APC), axin and glycogen synthase kinase 3β (GSK3β). β-Catenin is phosphorylated by GSK3β and degraded by a ubiquitin-proteasome pathway. In the presence of Wnt, however, the inactivation of the destruction complex leads to the translocation of β-catenin into the nucleus where it served as a cofactor for Tcf/Lef transcription factor. This sequential event transactivates the transcription of several target genes including cyclin D1.[24] To evaluate whether (*R*)-**4b** affects the activation of the Wnt signaling pathway, we determined the effect on the expression of β-catenin in A549 cells. (*R*)-**4b** suppressed the expression of β-catenin in A549 cells in a concentration-dependent manner (Fig. 3B). In addition, a reporter plasmid containing the Tcf transcription factor (TOPflash) binding site was indirectly determined in HEK293 cells to investigate whether the β-catenin suppression is associated with the inhibition of β-catenin-mediated transcriptional regulation or the β-catenin/Tcf transcriptional activity.[25] The β-catenin/Tcf transcriptional activity was remarkably activated by treatment with the plasmid of β-catenin and Tcf4 in HEK293 cells, whereas (*R*)-**4b** inhibited the elevated transcriptional activity in a concentration-dependent manner (Fig. 3C). Accordingly, the suppression of β-catenin and cyclin D1, one of the target genes of Wnt signaling, by (*R*)-**4b** correlated highly with the modulation of Wnt signaling pathway by (*R*)-**4b**.

2.5. Compound (*R*)-4b inhibits the growth of paclitaxel-resistant lung cancer cells

Although chemotherapy is the first line for treating late-stage cancer patients, drug resistance acquired by anticancer agents is a major therapeutic problem. One plausible common mechanism of anticancer drug resistance is associated with the overexpression

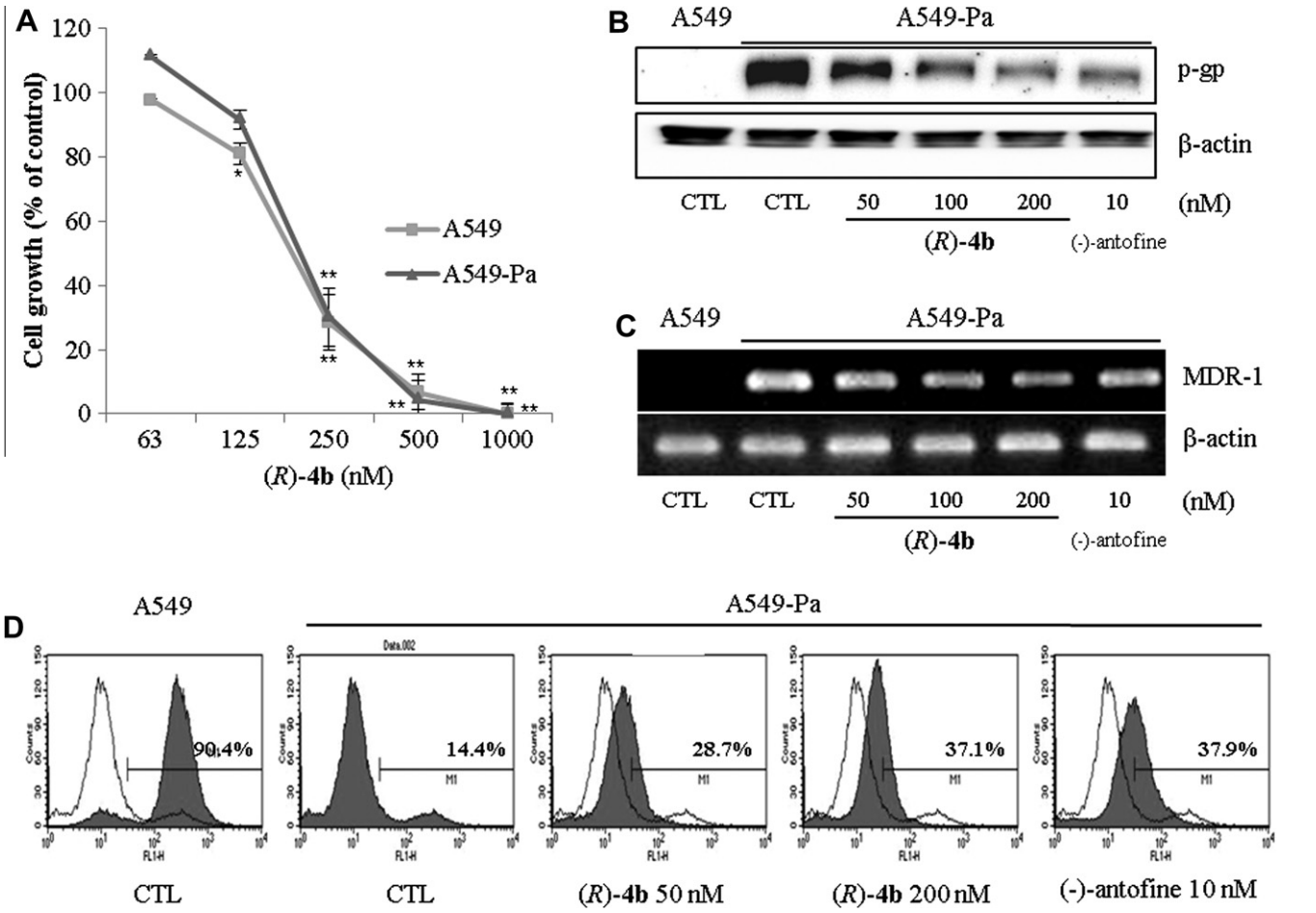

Figure 4. The effects of (*R*)-**4b** on paclitaxel-resistant A549-Pa cells. (**A**) The growth inhibition of (*R*)-**4b** in A549 cells. The cells were treated with (*R*)-**4b** for 72 h, and then the antiproliferative activity was evaluated by SRB assay. $^{*}p$ <0.05; $^{**}p$ <0.01, compared with the DMSO control. (**B**) The down-regulation of P-gp expression in A549-Pa cells. The A549-Pa cells were treated with (*R*)-**4b** and (−)-antofine for 48 h, and then the expression of P-gp was determined by Western blot analysis. The A549 cells were also analyzed the P-gp expression for comparison. (**C**) The suppression of MDR-1 gene expression in A549-Pa cells. The A549-Pa cells were treated with (*R*)-**4b** and (−)-antofine for 48 h, and then the gene expression of MDR-1 was determined by RT-PCR analysis. (**D**) The accumulation of intracellular rhodamine-123 dye following (*R*)-**4b** treatment in the A549-Pa cells. The cells were treated with (*R*)-**4b** and (−)-antofine for 72 h, and then the intracellular rhodamine-123 accumulation was measured using FACS analysis.

of P-glycoprotein (P-gp), an ATP-dependent transmembrane protein.[26] Therefore, P-gp causes the efflux pump to transport a variety of anticancer drugs from inside to outside of the cancer cells, which allows them to avoid the effects of the drug. In this line, we examined whether (*R*)-**4b** overcomes the resistance acquired by anticancer drugs. The anti-proliferative activity of (*R*)-**4b** was evaluated via the SRB assay of A549 and the paclitaxel-resistant human lung cancer cell line, A549-Pa, which was previously established to have an approximately 200-fold resistance by our group.[27] As shown in Figure 4A, (*R*)-**4b** exhibited almost equally potent growth inhibition in both the parent and paclitaxel-resistant cells (IC_{50} of (*R*)-**4b** = 200 nM for A549-Pa and 120 nM for A549). To further elucidate the mechanism of action leading to the ability to overcome paclitaxel resistance, we analyzed the modulations in the P-gp expression and function caused by (*R*)-**4b**. In accordance with previous reports,[27] the established A549-Pa cells showed a marked overexpression of P-gp relative to the parent A549 cells, which suggests the paclitaxel-resistance of A549-Pa cells was highly correlated to the acquired P-gp overexpression (Fig. 4B). However, the P-gp expression levels were suppressed by the treatment of A549-Pa cells with (*R*)-**4b** for 48 h. Additionally, we found that (*R*)-**4b** decreased the expression of the MDR-1 gene in the A549-Pa cells (Fig. 4C). These results suggest that the ability to overcome paclitaxel-resistance with (*R*)-**4b** could be related to the modulation of the transcriptional and translational level of P-gp expression. Moreover, (*R*)-**4b** also inhibited the efflux-pump activity of P-gp in the A549-Pa cells (Fig. 4D). These events suggest that (*R*)-**4b** might express the dual functions of down-regulating P-gp expression and inhibiting P-gp activity in the A549-Pa cells. These findings suggest an additional chemotherapeutic value of (*R*)-**4b**, that is, the regulation of cancer cell drug resistance.

2.6. Compound (*R*)-4b potentiates the inhibition of paclitaxel-resistant lung cancer cell growth in combination with anticancer drugs

Based on the potential down-regulation and functional inhibition of P-gp by (*R*)-**4b**, we evaluated whether combining (*R*)-**4b** with other anticancer agents, such as paclitaxel and gefitinib, enhances growth inhibition. Gefitinib was developed as the first selective inhibitor of epidermal growth factor receptor tyrosine kinase, and it is mainly used for lung cancer therapy.[28] Gefitinib was also reported to modulate the function of P-gp both in vitro and in vivo including the inhibitory activity of P-gp and potentiation of the action of known P-gp substrate cytotoxic drugs.[29] A549-Pa cells were plated (5×10^4 cells/mL) and treated with both (*R*)-**4b** (0–200 nM) and the anticancer drugs at the indicated concentrations for 48 h. The growth inhibition was determined using an SRB colorimetric assay. As shown in Figure 5, combining (*R*)-**4b**

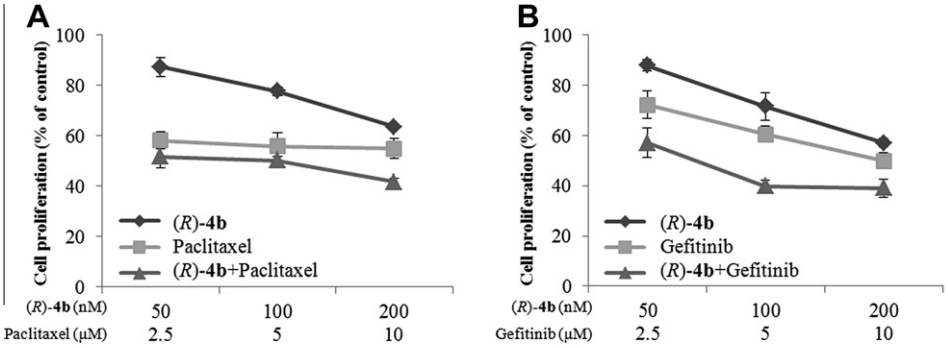

Dose (μM)		Combination index	Description
(*R*)-**4b**	Paclitaxel		
0.05	2.5	0.242	strong synergism
0.1	5	0.391	synergism
0.2	10	0.413	synergism

Dose (μM)		Combination index	Description
(*R*)-**4b**	Gefitinib		
0.05	2.5	0.653	synergism
0.1	5	0.523	synergism
0.2	10	1.002	additive

Figure 5. The growth inhibition of A549-Pa cells by (*R*)-**4b** combined with paclitaxel or gefitinib. The cells were treated with either (*R*)-**4b** alone or in combination with paclitaxel (**A**) or gefitinib (**B**) for 48 h, and then the antiproliferative activity was measured using an SRB assay.

with paclitaxel displayed a synergistic effect on growth inhibition (Fig. 5A). Additionally, combining (*R*)-**4b** with gefitinib also enhanced the growth inhibition of the A549-Pa cells relative to gefitinib treatment alone (Fig. 5B). These results suggest that the growth inhibition of (*R*)-**4b** in combination with paclitaxel or gefitinib could be due to the down-regulation of P-gp by (*R*)-**4b**.

2.7. In vivo antitumor effect of (*R*)-4b

Based on the high in vitro antiproliferative effect and high water solubility of (*R*)-**4b**, we performed studies using an in vivo tumor xenograft model bearing A549 and A549-Pa cells to further determine the anticancer potential of (*R*)-**4b**. When the tumor size reached approximately 100 mm^3, (*R*)-**4b** (5 or 10 mg/kg) was administered ip to mice three times per week. The tumor volume in the control group was approximately 1200 mm^3 and 1000 mm^3 for the A549 and A549-Pa cells, respectively, 35 days after the cells had been implanted. Relative to the tumor growth in control group, the growth of tumors after treating with (*R*)-**4b** was significantly inhibited. The inhibition rates of the tumor size relative to the control volume were 54.9% and 60.7% at 5 mg/kg and 10 mg/kg of (*R*)-**4b**, respectively, in the A549 cells bearing tumors (Fig. 6A). The tumor size inhibition rates in the A549-Pa cells bearing tumors were 38.4% and 54.8% at 5 mg/kg and 10 mg/kg of (*R*)-**4b**, respectively (Fig. 6B). The tumor weight was also significantly inhibited by the (*R*)-**4b** treatment of the A549 and A549-Pa tumor cells (Fig. 6C and 6D). In addition, the body weight change and overt toxicity were negligible for the (*R*)-**4b** treatment (data not shown). Immunohistochemical analysis of tumors using the Ki-67 antibody showed that (*R*)-**4b** inhibited the expression of the proliferation biomarker Ki-67 in the A549 and A549-Pa cells (Fig. 6E). The expression of P-gp in the A549-Pa bearing tumors was also dose-dependently suppressed by (*R*)-**4b** (Fig. 6F), which indicates (*R*)-**4b** overcomes the paclitaxel-resistance.

3. Conclusion

In an attempt to overcome the drawbacks of phenanthroindolizidine alkaloids, we designed and synthesized several antofine derivatives with a hydrophilic substituent at C-13a. Among these derivatives, the hydroxymethyl analogue (*R*)-**4b** exhibited notable antiproliferative activity in both cell cultures and in vivo tumor xenograft models against human lung cancer cells. Although (*R*)-**4b** was approximately tenfold less potent in vitro than the parent natural product, (−)-antofine, its thermodynamic aqueous solubility was at least 300 times higher. This significant solubility improvement could be ascribed to the increased hydrophilicity and disruption of the molecular planarity imparted by the substituent at C-13a. Cell cycle arrest and the suppression of the Akt/mTOR and Wnt signaling pathways have been shown to be a plausible mechanism of action for the antiproliferative activity of (*R*)-**4b**. These results suggest that (*R*)-**4b** is a promising new chemotherapeutic candidate with sufficient aqueous solubility, especially for managing lung cancer. In addition, the increased hydrophilicity of phenanthroindolizidine was expected to lower the BBB permeability level, which might potentially reduce the CNS toxicity. Further studies on the CNS side effects and metabolic behaviors of the present compound will be reported in due course.

4. Experimental

4.1. Chemistry

4.1.1. General

All chemicals were reagent grade and used as purchased. All reactions were performed under an inert atmosphere of dry nitrogen using distilled dry solvents. Reactions were monitored through TLC analysis using silica gel 60 F-254 thin layer plates. Compounds were visualized on the TLC plates under UV light and by spraying with either $KMnO_4$ or anisaldehyde solutions. Flash column chromatography was conducted on silica gel 60 (230–400 mesh). Melting points were measured using a Buchi B-540 melting point apparatus without correction. ^1H NMR (400 MHz) and ^{13}C NMR (75 or 100 MHz) spectra were recorded in δ units relative to the deuterated solvent. The IR spectra were measured on a Fourier Transform Infrared spectrometer. High-resolution mass spectra (HRMS) were recorded using EI or FAB. Purities of products were determined by HPLC peak area analysis (ZORBAX Eclipse plus

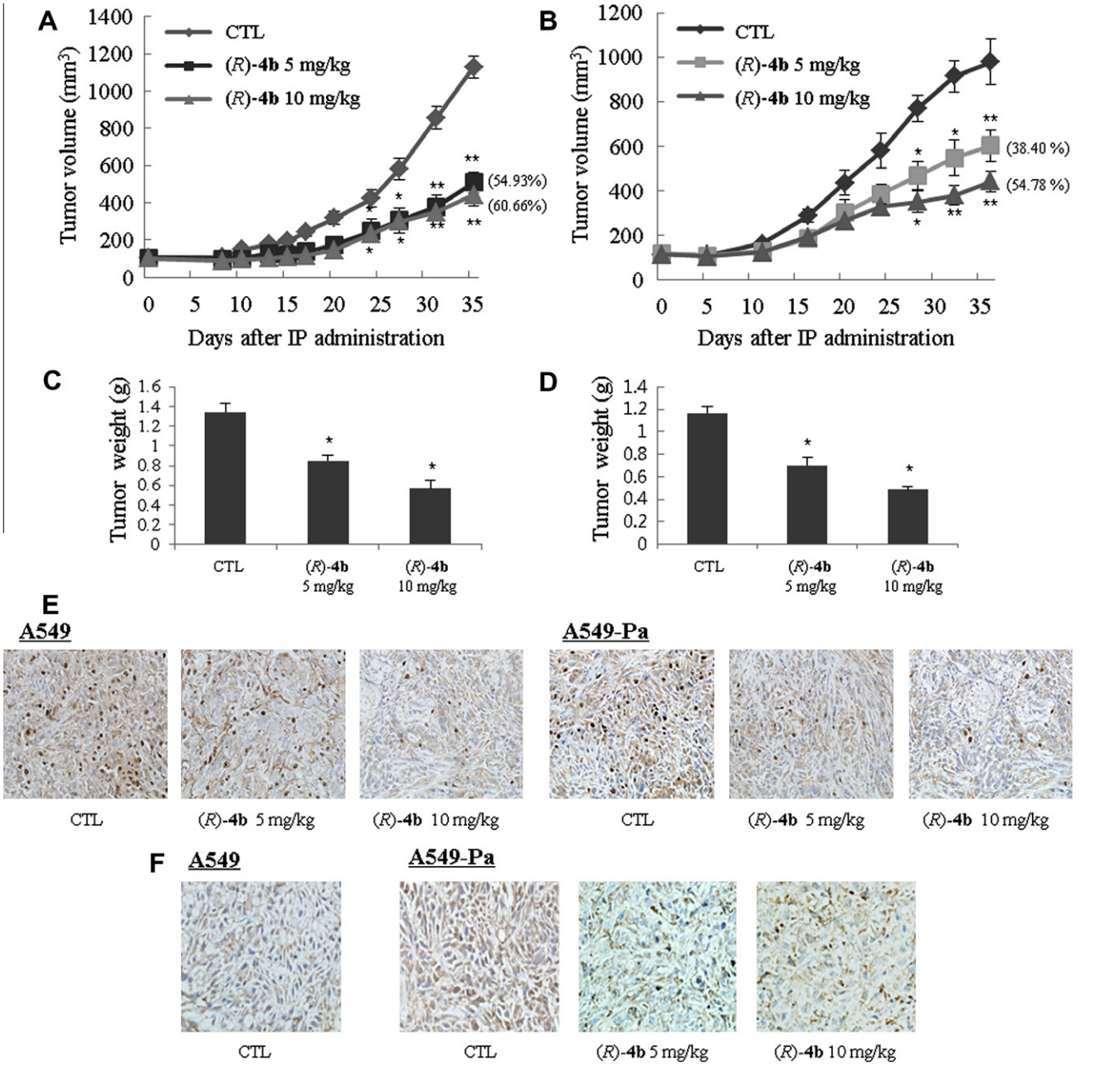

Figure 6. Antitumor effect of (*R*)-**4b** in a tumor xenograft model bearing A549 (A) and A549-Pa (B) cells. Cells were injected subcutaneously into the right flank of each mouse. When the tumor volume reached 95–100 mm^3, the mice were treated with (*R*)-**4b** (5 or 10 mg/kg/day) using intra-peritoneal injections 3 times per week. The tumor volumes were monitored every 3–5 days. At the end of the study, the tumors were excised and weighed (C) and (D). $^*p$ <0.05; $^{**}p$ <0.01, compared with the control. The tumor sections were also stained by immunohistochemistry for Ki-67 (E) and P-gp (**F**).

C18 column, 4.6 mm × 100 mm, 3.5 μm; flow rate of 0.7 mL/min; 30–100% aqueous MeOH with 0.1% formic acid over 20 min and MeOH with 0.1% formic acid from 20 to 25 min).

4.1.2. 1-*tert*-Butyl 2-methyl 2-((3,6,7-trimethoxyphenanthren-9-yl)methyl)pyrolidi-ne-1,2-dicarboxylate (8)

Diisopropylamine (266 μL, 1.88 mmol) was dissolved in THF (1.5 mL) and cooled to −78 °C before adding *n*-BuLi dropwise (1.6 M solution in hexane, 1.03 mL, 1.65 mmol). After this addition, the solution was stirred for 1 h at room temperature and then cooled to 0 °C. HMPA (326 μL, 1.87 mmol) was added dropwise, and the solution was stirred for 10 min at 0 °C. *N*-Boc-L-ProOMe (162 mg, 0.71 mmol) was dissolved in THF (1 mL) and added to the stirred solution. The resulting solution was stirred for 1 h at 0 °C. Phenanthryl bromide **7** (170 mg, 0.47 mmol) was dissolved in THF (3 mL) and added dropwise at 0 °C, and the reaction mixture was allowed to stir for 1 h at room temperature. The reaction was quenched with saturated aqueous NH_4Cl solution at 0 °C, diluted with H_2O, and extracted with EtOAc. The organic layer was dried with over $MgSO_4$ and concentrated in vacuo. The crude product was separated by silica gel column chromatography (hexane/EtOAc, 2:1) to give **8** (170 mg, 71%) as a yellow waxy solid (mixture of rotamer); ^{1}H NMR (400 MHz, $CDCl_3$) δ 1.40–1.46 (m, 2H), 1.51 (d, J = 16.8 Hz, 9H), 1.91–1.98 (m, 1H), 2.02–2.10 (m, 1H), 2.78–2.84 (m, 0.5H), 2.98–3.04 (m, 0.5H), 3.31–3.37 (m, 0.5H), 3.43–3.49 (m, 0.5H), 3.78 (d, J = 3.1 Hz, 3H), 3.76–4.05 (m, 2H), 3.99 (d, J = 0.9 Hz, 3H), 4.03 (d, J = 3.0 Hz, 3H), 4.09 (s, 3H), 7.15–7.19 (m, 1H), 7.40 (d, J = 4.9 Hz, 1H), 7.55 (d, J = 23.7 Hz, 1H), 7.69 (t, J = 8.7 Hz, 1H), 7.82

(s, 1H), 7.90 (d, J = 4.2 Hz, 1H); ^{13}C NMR (75 MHz, $CDCl_3$) δ 22.5, 23.0, 28.4, 28.6, 34.3, 35.7, 36.8, 48.0, 48.1, 52.4, 55.6, 56.0, 56.06, 56.1, 69.1, 69.5, 79.8, 80.4, 103.8, 104.0, 105.6, 105.9, 115.5, 124.6, 124.7, 125.9, 126.0, 127.9, 128.0, 128.1, 128.2, 128.5, 128.8, 129.0, 129.7, 130.0, 130.3, 148.6, 148.7, 149.4, 149.5, 153.6, 154.6, 158.0, 158.2, 175.3, 175.5; IR (KBr, cm^{-1}) ν_{max} 2974, 1739, 1693, 1525, 1390, 1268, 1162, 755; HRMS (FAB) calcd for $C_{29}H_{35}NO_7$ ([M]$^+$) 509.2414, found 509.2414.

4.1.3. 2,3,6-Trimethoxy-9,11,12,13-tetrahydro-10*H*-9a-aza-cyclopenta[*b*]triphenyle-ne-12a-carboxylic acid methyl ester (4a)

A solution of **8** (60 mg, 0.12 mmol) and formaldehyde (37%, 2 mL) in EtOH (8 mL) was acidified with concentrated HCl (200 μL). The mixture was refluxed for 21 h in the dark and concentrated to dryness under reduced pressure. The residue was dissolved in CH_2Cl_2 (40 mL) and treated with 10% NaOH (20 mL). The aqueous layer was extracted with CH_2Cl_2 (2 × 30 mL) and the combined organic extracts were washed with water and brine before dryied over $MgSO_4$, filtered and concentrated in vacuo. Purification of the residue by flash column chromatography on silica gel (CH_2Cl_2/MeOH, 40:1) afforded the desired product **4a** (42.3 mg, 85%) as a white solid; mp 204–206 °C; ^{1}H NMR (400 MHz, $CDCl_3$) δ 1.98–2.14 (m, 3H), 2.32–2.38 (m, 1H), 2.96 (d, J = 15.9 Hz, 1H), 3.23 (q, J = 7.4 Hz, 1H), 3.32 (q, J = 7.5 Hz, 1H), 3.53 (s, 3H), 3.85 (d, J = 15.9 Hz, 1H), 3.98 (s, 3H), 4.07 (s, 3H), 4.08 (s, 3H), 4.46 (dd, J = 16.0 Hz, 26.2 Hz, 2H), 7.18 (dd, J = 2.3 Hz, 9.0 Hz, 1H), 7.33 (s, 1H), 7.80 (d, J = 9.0 Hz, 1H), 7.87 (d, J = 2.2 Hz, 1H), 7.89 (s, 1H); ^{13}C NMR (100 MHz, $CDCl_3$) δ 21.0, 33.6, 37.5, 47.8, 51.3, 51.7, 55.5, 55.9, 56.0, 66.1, 103.9, 104.7, 114.8, 123.6, 123.9, 124.0, 124.4, 125.9, 126.8, 130.2, 148.4, 149.4, 157.6, 175.2; IR (KBr, cm^{-1}) ν_{max} 1622, 1512, 1256, 1208, 1130, 1038; HRMS (FAB) calcd for $C_{25}H_{28}NO_5$ ([M+H]$^+$) 422.1967, found 422.1977; purity by HPLC: 96.9%.

4.1.4. (2,3,6-Trimethoxy-9,11,12,13-tetrahydro-10*H*-9a-aza-cyclopenta[*b*]triphenyl-en-12a-yl)-methanol (4b)

$LiAlH_4$ (160 μL, 1.0 M solution in THF, 0.16 mmol) was added to a solution of the methyl ester analogue **4a** (31.5 mg, 0.07 mmol) in dry THF (1.5 mL) at 0 °C. After 20 min, the solution was warmed to rt over 1 h. The reaction was quenched with 10% NaOH solution at 0 °C. The suspension was then filtered over a Celite pad, and the filtrate was concentrated in vacuo. Purification of the residue by flash column chromatography on silica gel (CH_2Cl_2/MeOH, 15:1) afforded the desired product **4b** (19.2 mg, 88%) as a light yellow solid; mp 183–185 °C; ^{1}H NMR (400 MHz, $CDCl_3$) δ 1.64–1.69 (m, 1H), 1.71–1.78 (m, 1H), 1.92–1.99 (m, 1H), 2.15–2.21 (m, 1H), 2.73 (q, J = 9.0 Hz, 1H), 2.90 (d, J = 16.5 Hz, 1H), 3.10 (d, J = 16.6 Hz, 1H), 3.42 (t, J = 8.4 Hz, 1H), 3.69 (t, J = 11.5 Hz, 2H), 4.00 (s, 3H), 4.06 (s, 3H), 4.09 (s, 3H), 4.31 (d, J = 16.4 Hz, 1H), 4.55 (d, J = 16.4 Hz, 1H), 7.21–7.24 (m, 1H), 7.29 (s, 1H), 7.81 (d, J = 9.0 Hz, 1H), 7.90 (d, J = 2.1 Hz, 1H), 7.92 (s, 1H); ^{13}C NMR (75 MHz, $CDCl_3$) δ 21.2, 28.7, 34.1, 45.8, 52.9, 55.6, 56.0, 56.1, 64.2, 103.5, 104.0, 105.0, 115.3, 123.0, 123.8, 124.0, 124.1, 126.2, 130.2, 148.9, 149.8, 157.9; IR (KBr, cm^{-1}) ν_{max} 1622, 1512, 1256, 1208, 1130, 1038; HRMS (FAB) calcd for $C_{24}H_{28}NO_4$ ([M+H]$^+$) 394.2018, found 394.2011; purity by HPLC: 96.0%.

4.1.5. 2,3,6-Trimethoxy-9,11,12,13-tetrahydro-10*H*-9a-aza-cyclopenta[*b*]triphenyle-ne-12a-carboxylic acid (4c)

A 1 N LiOH solution (0.3 mL) was added to a solution of **4a** (21 mg, 0.05 mmol) in THF (2 mL) and refluxed overnight in the dark. The reaction mixture was cooled to room temperature and filtered over a Celite pad, and the filtrate was concentrated in vacuo. The resulting residue was purified by silica gel column chromatography (CH_2Cl_2/MeOH, 8:1) to afford the desired product **4c** (19.2 mg, 81%) as a white solid; mp 207–219 °C; ^{1}H NMR (400 MHz, $CDCl_3$ + CD_3CO_2D) δ 1.66–1.70 (m, 2H), 1.80–1.81 (m, 1H), 2.61–2.70 (m, 2H), 3.03 (d, J = 15.7 Hz, 1H), 3.48 (d, J = 15.8 Hz, 1H) 3.81 (s, 3H), 3.87 (s, 3H), 3.87–3.92 (m, 2H), 4.10 (s, 3H), 4.25 (d, J = 14.3 Hz, 1H), 7.19 (d, J = 8.5 Hz, 1H), 7.45 (s, 1H), 7.54 (d, J = 15.3 Hz, 2H), 7.69 (d, J = 9.0 Hz, 1H); ^{13}C NMR (75 MHz, $CDCl_3$ + CD_3CO_2D) δ 23.1, 30.7, 35.9, 46.6, 55.2, 55.4, 55.8, 56.3, 75.0, 103.5, 104.2, 104.6, 121.5, 122.9, 124.25, 124.32, 125.1, 127.3, 130.3, 149.7, 150.3, 158.3, 173.8; IR (KBr, cm^{-1}) ν_{max} 3414, 3007, 1618, 1518, 1260, 1205, 1027, 755; HRMS (FAB) calcd for $C_{24}H_{26}NO_5$ ([M+H]$^+$) 408.1811, found 408.1813; purity by HPLC: 99.3%.

4.1.6. (3*R*,7a*R*)-3-Trichloromethyl-7a-(3,6,7-trimethoxy-phenanthren-9-ylmethyl)-tetrahydro-pyrrolo[1,2-*c*]oxazol-1-one ((*R*,*R*)-10)

n-BuLi (1.6 M solution in hexane, 7.5 mL, 12 mmol) was added to a stirred solution of diisopropylamine (1.7 mL, 12 mmol) in dry THF (23 mL), at −78 °C under N_2. The solution was allowed to warm to room temperature before stirring for 1 hour. This solution was added dropwise to oxazolidinone (3*R*,7a*S*)-**9** (2.00 g, 8.18 mmol) in dry THF (6 mL) at −78 °C over 20 min (reaction mixture turned dark), stirred for another 30 min, and then phenanthryl bromide **7** (1.2 g, 3.32 mmol) was added dropwise over 10 min. The solution warmed to −40 °C over 4 h. The reaction was quenched with a saturated NH_4Cl solution and extracted with chloroform (3 × 40 mL). The combined organic layers were washed with brine (25 mL), dried over $MgSO_4$, filtered, and concentrated in vacuo. Purification of the residue by flash column chromatography on silica gel (hexane/EtOAc, 5:1) afforded oxazolidinone (*R*,*R*)-**10** (1.24 g, 71%) as a white solid; mp 226–229 °C; $[\alpha]_D^{24}$ +4.0 (*c* 0.25, $CHCl_3$); ^{1}H NMR (400 MHz, $CDCl_3$) δ 1.20–1.26 (m, 1H), 1.41–1.48 (m, 1H), 2.02 (dd, J = 5.8 Hz, 8.4 Hz, 2H), 2.70–2.77 (m, 1H), 2.97–3.02 (m, 1H), 3.67 (dd, J = 14.7 Hz, 18.4 Hz, 2H), 4.00 (s, 3H), 4.07 (s, 3H), 4.10 (s, 3H), 5.02 (s, 1H), 7.18 (dd, J = 2.2 Hz, 8.7 Hz, 1H), 7.61 (s, 1H), 7.69 (s, 1H), 7.74 (d, J = 8.8 Hz, 1H), 7.82 (s 1H), 7.90 (s, 1H); ^{13}C NMR (100 MHz, $CDCl_3$) δ 25.0, 34.8, 38.8, 55.6, 56.0, 56.4, 58.2, 73.5, 100.6, 102.8, 103.75, 103.79, 105.7, 115.6, 124.7, 125.8, 127.2, 127.6, 128.7, 130.0, 130.6, 148.8, 149.6, 158.3, 176.7; IR (KBr, cm^{-1}) ν_{max} 2958, 1608, 1387, 1355, 1115, 1034, 839, 792; HRMS (FAB) calcd for $C_{25}H_{24}Cl_3NO_5$ ([M]$^+$) 523.0720, found 523.0741.

4.1.7. (3*S*,7a*S*)-3-Trichloromethyl-7a-(3,6,7-trimethoxy-phenanthren-9-ylmethyl)-tetrahydro-pyrrolo[1,2-*c*]oxazol-1-one ((*S*,*S*)-10)

Compound (*S*,*S*)-**10** was prepared from **7** and (3*S*,7a*R*)-**7** in 71% yield using a procedure similar to that for compound (*R*,*R*)-**10**. White solid; $[\alpha]_D^{24}$ −2.5 (*c* 1.55, $CHCl_3$). All spectral data were in accordance with (*R*,*R*)-**10**.

4.1.8. (*R*)-2-(3,6,7-Trimethoxy-phenanthren-9-ylmethyl)-pyrrolidine-2-carboxylic acid methyl ester ((*R*)-11)

Acetyl chloride (350 μL, 4.96 mmol) was added to a solution of oxazolidinone (*R*,*R*)-**10** (650 mg, 1.24 mmol) in dry MeOH (12 mL) at 0 °C. The reaction mixture was refluxed for 2 days before concentrating in vacuo. The residue was dissolved in CH_2Cl_2 and treated with 1 M NaOH. The aqueous layer was extracted with CH_2Cl_2 (2 × 20 mL), and the combined organic extracts were washed with brine (10 mL), dried over $MgSO_4$, filtered, and concentrated in vacuo. Purification of the residue by flash column chromatography on silica gel (CH_2Cl_2/MeOH, 25:1) afforded the desired product, methyl ester amine (*R*)-**11** (366 mg, 72%), as a light brown solid; mp 174–178 °C; $[\alpha]_D^{24}$ +33.1 (*c* 0.25, $CHCl_3$); ^{1}H NMR (400 MHz, $CDCl_3$) δ 1.64–1.72 (m, 1H), 1.77–2.02 (m, 3H), 2.37 (ddd, J = 4.6 Hz, 8.3 Hz, 12.8 Hz, 1H), 2.90 (td, J = 6.5 Hz, 9.0 Hz, 1H), 3.02 (ddd, J = 5.6 Hz, 7.7 Hz, 9.6 Hz, 1H), 3.38 (s, 3H), 3.38 (d, J = 14.0 Hz, 1H), 3.59 (d, J = 14.2 Hz, 1H), 3.99 (s, 3H), 4.06 (s, 3H), 4.09 (s, 3H), 7.16 (dd, J = 2.3 Hz, 8.7 Hz, 1H), 7.48 (s, 1H), 7.62 (s,

1H), 7.72 (d, J = 8.8 Hz, 1H), 7.81 (d, J = 2.1 Hz, 1H), 7.88 (s, 1H); ^{13}C NMR (100 MHz, $CDCl_3$) δ 24.2, 35.7, 42.0, 45.8, 52.1, 55.6, 55.9, 56.0, 70.9, 103.7, 103.8, 106.0, 115.4, 124.6, 125.9, 126.5, 127.3, 128.9, 129.9, 130.5, 148.5, 149.0, 158.1, 177.1; IR (KBr, cm^{-1}) ν_{max} 1622, 1512, 1256, 1208, 1130, 1038; HRMS (FAB) calcd for $C_{24}H_{28}NO_5$ ($[M+H]^+$) 410.1967, found 410.1980.

4.1.9. (*S*)-2-(3,6,7-Trimethoxy-phenanthren-9-ylmethyl)-pyrrolidine-2-carboxylic acid methyl ester ((*S*)-11)

Compound (*S*)-**11** was prepared from (*S*,*S*)-**10** in a 73% yield using a procedure similar to that for compound (*R*)-**11**. Light brown solid; $[\alpha]_D^{24}$ −30.4 (*c* 0.35, $CHCl_3$). All spectral data were in accordance with (*R*)-**11**.

4.1.10. (*R*)-2,3,6-Trimethoxy-9,11,12,13-tetrahydro-10*H*-9a-aza-cyclopenta[*b*]triph-enylene-12a-carboxylic acid methyl ester ((*R*)-4a)

A solution of methyl ester amine (*R*)-**11** (120 mg, 0.29 mmol) and formaldehyde (37%, 2 mL) in EtOH (10 mL) was acidified with concentrated HCl (250 μL). The mixture was stirred at reflux for 21 h in the dark. The reaction mixture was concentrated to dryness under reduced pressure. The residue was dissolved in CH_2Cl_2 (40 mL) and treated with 1 M NaOH (20 mL). The aqueous layer was extracted with CH_2Cl_2 (2 × 30 mL) and the combined organic extracts were washed with water and brine before dried over $MgSO_4$, filtered, and concentrated in vacuo. Purification of the residue by flash column chromatography on silica gel (CH_2Cl_2/MeOH, 40:1) afforded the desired product (*R*)-**4a** (98 mg, 80%) as a white solid; mp 204–206 °C; $[\alpha]_D^{24}$ −87.4 (*c* 1.00, $CHCl_3$); ^{1}H NMR (400 MHz, $CDCl_3$) δ 1.98–2.14 (m, 3H), 2.32–2.38 (m, 1H), 2.96 (d, J = 15.9 Hz, 1H), 3.23 (q, J = 7.4 Hz, 1H), 3.32 (q, J = 7.5 Hz, 1H), 3.53 (s, 3H), 3.85 (d, J = 15.9 Hz, 1H), 3.98 (s, 3H), 4.07 (s, 3H), 4.08 (s, 3H), 4.46 (dd, J = 16.0 Hz, 26.2 Hz, 2H), 7.18 (dd, J = 2.3 Hz, 9.0 Hz, 1H), 7.33 (s, 1H), 7.80 (d, J = 9.0 Hz, 1H), 7.87 (d, J = 2.2 Hz, 1H), 7.89 (s, 1H); ^{13}C NMR (100 MHz, $CDCl_3$) δ 21.0, 33.6, 37.5, 47.8, 51.3, 51.7, 55.5, 55.9, 56.0, 66.1, 103.9, 104.7, 114.8, 123.6, 123.9, 124.0, 124.4, 125.9, 126.8, 130.2, 148.4, 149.4, 157.6, 175.2; IR (KBr, cm^{-1}) ν_{max} 1622, 1512, 1256, 1208, 1130, 1038; HRMS (FAB) calcd for $C_{25}H_{28}NO_5$ ($[M+H]^+$) 422.1967, found 422.1977.

4.1.11. (*S*)-2,3,6-Trimethoxy-9,11,12,13-tetrahydro-10*H*-9a-aza-cyclopenta[*b*]triph-enylene-12a-carboxylic acid methyl ester ((*S*)-4a)

Compound (*S*)-**4a** was prepared from (*S*)-**11** in 78% yield using a procedure similar to that for compound (*R*)-**4a**. White solid; $[\alpha]_D^{24}$ +99.6 (*c* 0.9, $CHCl_3$). All spectral data were in accordance with (*R*)-**4a**.

4.1.12. (*R*)-(2,3,6-Trimethoxy-9,11,12,13-tetrahydro-10*H*-9a-aza-cyclopenta[*b*]trip-henylen-12a-yl)-methanol ((*R*)-4b)

$LiAlH_4$ (290 μL, 1.0 M in THF, 0.29 mmol) was added to a solution of the methyl ester analogue (*R*)-**4a** (80 mg, 0.19 mmol) in dry THF (4 mL) at 0 °C. After 20 min, the solution was warmed to rt over 1 h. The reaction was quenched with a 10% NaOH solution at 0 °C. The suspension was then filtered over a Celite pad, and the filtrate was concentrated in vacuo. Purification of the residue by flash column chromatography on silica gel (CH_2Cl_2/MeOH, 15:1) afforded the desired product (*R*)-**4b** (68 mg, 91%) as a light yellow solid; mp 183–185 °C; $[\alpha]_D^{24}$ −39.0 (*c* 0.46, $CHCl_3$); ^{1}H NMR (400 MHz, $CDCl_3$) δ 1.64–1.69 (m, 1H), 1.71–1.78 (m, 1H), 1.92–1.99 (m, 1H), 2.15–2.21 (m, 1H), 2.73 (q, J = 9.0 Hz, 1H), 2.90 (d, J = 16.5 Hz, 1H), 3.10(d, J = 16.6 Hz, 1H), 3.42 (t, J = 8.4 Hz, 1H), 3.69 (t, J = 11.5 Hz, 2H), 4.00 (s, 3H), 4.06 (s, 3H), 4.09 (s, 3H), 4.31 (d, J = 16.4 Hz, 1H), 4.55 (d, J = 16.4 Hz, 1H), 7.21–7.24 (m, 1H), 7.29 (s, 1H), 7.81 (d, J = 9.0 Hz, 1H), 7.90 (d, J = 2.1 Hz, 1H), 7.92 (s, 1H); ^{13}C NMR (75 MHz, $CDCl_3$) δ 21.2, 28.7, 34.1, 45.8, 52.9, 55.6, 56.0, 56.1, 64.2, 103.5, 104.0, 105.0, 115.3, 123.0, 123.8, 124.0, 124.1, 126.2, 130.2, 148.9, 149.8, 157.9; IR (KBr, cm^{-1}) ν_{max} 1622, 1512, 1256, 1208, 1130, 1038; HRMS (FAB) calcd for $C_{24}H_{28}NO_4$ ($[M+H]^+$) 394.2018, found 394.2011; purity by HPLC: 95.6%.

4.1.13. (*S*)-(2,3,6-Trimethoxy-9,11,12,13-tetrahydro-10*H*-9a-aza-cyclopenta[*b*]triph-enylen-12a-yl)-methanol ((*S*)-4b)

Compound (*S*)-**4b** was prepared from (*S*)-**4a** in 91% yield using a procedure similar to that for compound (*R*)-**4b**. Light yellow solid; $[\alpha]_D^{24}$ +41.3 (*c* 0.35, $CHCl_3$). All spectral data were in accordance with (*R*)-**4b**; purity by HPLC: 95.1%.

4.2. Biology

4.2.1. Growth inhibition assay

The growth-inhibitory potential of the test compounds against various human cancer cells was determined by SRB assay. Cells were seeded in 96-well plates at a density of 5×10^3 cells/well and treated with various concentrations of the test compounds for 72 h. The cells were fixed with a 10% trichloroacetic acid solution for 30 min at 4 °C, washed 5 times with tap water, and dried in the air. The cells were stained with 0.4% SRB solution in 1% acetic acid for 30 min at room temperature. After washing out the unbound dye and drying, the stained cells were dissolved in 10 mM Tris (pH 10.0), and the absorbance was measured at 515 nm. Cell viability was calculated by comparing to the absorbance of the vehicle-treated control group. The IC_{50} values, the concentration for 50% cell survival, were determined via non-linear regression analysis using Table curve software.

4.2.2. Analysis of cell cycle distribution

The cell cycle dynamic was measured via flow cytometric analysis. A549 cells (3.6×10^5 cells/dish in 60 mm dishes) were incubated with test samples for 24 h. All adhering and floating cells were collected and washed twice with PBS before being fixed with 100% methanol overnight. The fixed cells were washed with PBS and stained with a 50 μg/mL propidium iodide (PI) solution containing 50 μg/ml RNase A for 30 min at room temperature. The fluorescence intensity was analyzed using a FACSCalibur® flow cytometer (BD Biosciences, San Jose, CA, USA). The percent distributions for the distinct cell cycle phases were determined using ModFIT LT V2.0 software.

4.2.3. Western blot analysis

Cultured A549 cells were seeded into 60 mm dishes at a density of 3×10^5 cells/dish and incubated for 24 h. These cells were treated with various concentrations of the test compounds for 24 h. After harvesting, the cells were washed twice with PBS, suspended by boiling 2× the sample loading buffer (250 mM Tris–HCl (pH 6.8), 4% SDS, 10% glycerol, 0.006% bromophenol blue, 2% β-mercaptoethanol, 50 mM sodium fluoride, and 5 mM sodium orthovanadate) and incubated for an additional 5–20 min at 100 °C for complete lysis. After cooling to room temperature, the samples were stored at −20 °C until use. The protein concentration of the cell lysates was determined via the BCA method. Equal amounts (25–50 μg) of protein samples were subjected to 8–15% SDS–PAGE. The separated proteins were electrically transferred onto polyvinylidene fluoride (PVDF) membranes (Millipore, Bedford, MA, USA) that were blocked with a blocking buffer (5% non-fat dry milk in PBS containing 0.1% Tween-20 (PBST)) for 1 h at room temperature. After washing 3 times with PBST, the membranes were incubated with primary antibodies diluted in 3% non-fat dry milk in PBS (1:1000–1:2000) overnight at 4 °C. These membranes were then washed 3 times with PBST and incubated with the corresponding secondary antibodies diluted in 3% non-fat dry

milk in PBS (1:2000–1:5000) for 1–2 h at room temperature. The membranes were washed 3 times with PBST again and exposed to an enhanced chemiluminescence (ECL) detection kit (LabFrontier, Suwon, Korea). The blots were detected using a LAS 3000 (Fuji Film Corp., Tokyo, Japan).

4.2.4. Reporter gene assay

HEK293 cells were co-transfected using 100 ng of TOPflash (β-catenin/Tcf reporter plasmids, Millipore, Billerica, MA, USA) and 5 ng of pRL-SV40 reporter plasmids for 24 h. After transfection, the cells were incubated with various concentrations of (*R*)-**4b** for 24 h. The luciferase activity was measured using a dual-luciferase reporter gene assay system. The transfection efficiency was normalized based on the *Renilla* luciferase activity.

4.2.5. Evaluation of the mRNA expression by RT-PCR

A549/A549-Pa cells (1×10^5 cells/dish in 100 mm dishes) were treated with (*R*)-**4b** for the indicated times. After incubation, the cells were washed twice with PBS and lysed with TRI® reagent. The RNA was extracted with chloroform, and the isolated RNA was precipitated with isopropyl alcohol. The RNA pellet was washed with 70% ethanol, air-dried, and dissolved in nuclease-free water. The absorbance was measured at 260 and 280 nm to determine the concentration and purity of the RNA. The total RNA (1 μg) was reverse transcribed using AMV reverse transcriptase and oligo $(dT)_{15}$ primer.

A polymerase chain reaction (PCR) was performed in a reaction mixture containing cDNA, a 0.2 mM dNTP mixture, 10 pmol of mdr1-specific primers (forward: 5′-CCCATCATTGCAATAGCAGG-3′, reverse: 5′-GTTCAAACTTCTGCTCCTGA-3′), and 0.25 U of Taq DNA polymerase using a GeneAmp PCR system 2400 (Applied Biosystems, Foster, CA, USA). Each of the PCR steps was generally performed as follows: initial denaturation for 4 min at 94 °C; 35 cycles amplification steps consisting of denaturation for 30 s at 94 °C, annealing for 30 s at 55 °C, and elongation for 30 s at 72 °C; and a final extension step for 5 min at 72 °C. The PCR products were separated by 2% agarose gel electrophoresis. The gel was stained with a 10,000-fold-diluted SYBR safe staining solution and visualized under a UV transilluminator (Alpha ImagerTM, Alpha Innotech Corp., USA).

4.2.6. Rhodamine-123 accumulation assay

A549/A549-Pa cells were seeded in 30 mm dishes at a density of 1×105 cells/dish. The cells were pretreated with the test compounds for 72 h. After pretreatment, the cells were incubated with 1 μg/mL of rhodamine-123 (Rh-123) in the culture medium at 37 °C and 5% CO_2 in the dark for 90 min. After Rh-123 accumulation, the cells were trypsinized from the subconfluent monolayer of cells, and the cell pellet was washed twice with ice-cold PBS. The cells were then immediately analyzed using a FACS Caliber® (BD Biosciences, San Jose, CA, USA) equipped with a 488 nm argon laser. The green fluorescence of Rh-123 was measured using a 530 nm band-pass filter.[30]

4.2.7. Analysis of combination index

Cells were plated in 96-well plates (5×10^4 cells/well) with various concentrations of test compounds. After 48 h of incubation, the growth inhibition was measured using the SRB assay. The combined effect of the test compounds was analyzed by calculating the combination index (CI) using the equation $CI = D_1/(D_x)_1 + D_2/(D_x)_2$, where D_1 and D_2 are the concentrations of the combined compounds that achieve the expected effect, and $(D_x)_1$ and $(D_x)_2$ are the concentrations that achieve similar effects when the compounds are used alone. In this study, 50% inhibition was chosen as the effective level. The calculated CI was then compared to reported reference values.[31]

4.2.8. In vivo antitumor activity in xenograft model

Six week-old female athymic mice (BALB/c nu/nu) were purchased from Orient Co., Ltd. (Seoul, Korea). An A549 or A549-Pa cell suspension (2×10^6 cells in 0.1 mL of RPMI) was injected subcutaneously into the right flank of each mouse on day 0. The mice were treated when their tumor volume reached 95–100 mm^3. The animals were randomly divided into three groups (five animals per group). (*R*)-**4b** (2 or 10 mg/kg body weight) dissolved in 1% cremophore in PBS was administered intraperitoneally three times a week. The control group was treated with an equal volume of the vehicle. The tumor volume was monitored three times per week for 35–39 days using calipers and estimated using the following formula: tumor volume (mm^3) = (width) × (length) × (height) × π/6. The body weight of each mouse was also monitored for toxicity.

4.2.9. Immunohistochemistry of tumor xenografts

The immunohistochemical analysis of tumor tissues was conducted to detect cell proliferation and drug-resistant biomarkers using the Ki-67 and P-pg antibodies, respectively. Sections of the tumor tissues were incubated at 4 °C overnight with the antibodies for Ki-67 and p-glycoprotein, detected using the EnVision Plus/HRP detection system (Dako, Carpinteria, CA, USA), and counterstained with hematoxylin. The stained section was observed under an inverted phase-contrast microscope and photographed.

4.2.10. Statistical analysis

Data were presented as the means ± S.D. for the indicated number of independently performed experiments. The statistical significance was analyzed using Student's *t*-test. Values with $p < 0.05$ were considered statistically significant.

Acknowledgements

This work was supported by a National Research Foundation of Korea (NRF) grant funded by the Korean Government (MOEHRD) (KRF-2010-0027312). This work was also supported by NRF grant funded by Korean Government (NRF-2012-Fostering Core Leaders of the Future Basic Science Program).

Supplementary data

Supplementary data associated with this article can be found, in the online version, at http://dx.doi.org/10.1016/j.bmc.2012.11.039.

References and notes

1. (a) Gellert, E. In *Alkaloids: Chemical and Biological Perspectives*; Pelletier, S. W., Ed.; Academic Press: New York, 1987; pp 55–132; (b) Suffness, M.; Cordell, G. A. In *The Alkaloids, Chemistry and Pharmacology*; Brossi, A., Ed.; Academic Press: New York, 1985; Vol. 25, pp 3–355.
2. Gellert, E. *J. Nat. Prod.* **1982**, *45*, 50.
3. Staerk, D.; Lykkeberg, A. K.; Christensen, J.; Budnik, B. A.; Abe, F.; Jaroszewski, J. W. *J. Nat. Prod.* **2002**, *65*, 1299.
4. Lee, S. K.; Nam, K.-A.; Heo, Y.-H. *Planta Med.* **2003**, *69*, 21.
5. Chemler, S. R. *Curr. Bioact. Compd.* **2009**, *5*, 2.
6. For recent reviews, see (a) Michael, J. P. *Nat. Prod. Rep.* **2008**, *25*, 139; (b) Michael, J. P. *Nat. Prod. Rep.* **2007**, *24*, 191; (c) Michael, J. P. *Nat. Prod. Rep.* **2005**, *22*, 603; (d) Li, Z.; Jin, Z.; Huang, R. *Synthesis* **2001**, *16*, 2365.
7. For recent representative examples, see: (a) Yang, X.; Shi, Q.; Lai, C.-Y.; Chen, C.-Y.; Ohkoshi, E.; Yang, S.-C.; Wang, C.-Y.; Bastow, K. F.; Wu, T.-S.; Pan, S.-L.; Teng, C.-M.; Yang, P.-C.; Lee, K.-H. *J. Med. Chem.* **2012**, *55*, 6751; (b) Yang, X.; Shi, Q.; Yang, S.-C.; Chen, C.-Y.; Yu, S.-L.; Bastow, K. F.; Morris-Natschke, S. L.; Wu, P.-C.; Lai, C.-Y.; Wu, T.-S.; Pan, S.-L.; Teng, C.-M.; Lin, J.-C.; Yang, P.-C.; Lee, K.-H. *J. Med. Chem.* **2011**, *54*, 5097; (c) Ikeda, T.; Yaegashi, T.; Matsuzaki, T.; Yamazaki, R.; Hashimoto, S.; Sawada, S. *Bioorg. Med. Chem. Lett.* **2011**, *21*, 5978; (d) Wang, K.; Wang, W.; Wang, Q.; Huang, R. *Lett. Org. Chem.* **2008**, *5*, 383; (e) Su, C.-R.; Damu, A. G.; Chiang, P.-C.; Bastow, K. F.; Morris-Natschke, S. L.; Lee, K.-H.; Wu, T.-S. *Bioorg. Med. Chem.* **2008**, *16*, 6233; (f) Gao, W.; Bussom, S.; Grill, S. P.; Gullen, E. A.; Hu, Y.-C.; Huang, X.; Zhong, S.; Kaczmarek, C.; Gutierrez, J.; Francis, S.; Baker, D. C.; Yu, S.; Cheng, Y.-C. *Bioorg. Med. Chem. Lett.* **2007**, *17*, 4338; (g) Fu, Y.; Lee, S. K.; Min, H.-Y.; Lee, T.; Lee, J.; Cheng, M.; Kim, S. *Bioorg.*

Med. Chem. Lett. **2007**, *17*, 97; (h) Chuang, T.-H.; Lee, S.-J.; Yang, C.-W.; Wu, P.-L. *Org. Biomol. Chem.* **2006**, *4*, 860.
8. Suffness, M.; Douros, J. In *Anticancer Agents Based on Natural Product Models*; Cassady, J. M., Douros, J. D., Eds.; Academic Press: London, 1980; pp 465–487.
9. Gopalakrishnan, C.; Shankaranarayan, D.; Kameswaran, L.; Natarajan, S. *Indian J. Med. Res.* **1979**, *69*, 513.
10. Hitchcock, S. A.; Pennington, L. D. *J. Med. Chem.* **2006**, *49*, 7559.
11. Ishikawa, M.; Hashimoto, Y. *J. Med. Chem.* **2011**, *54*, 1539.
12. (a) Log BB was calculated using the following equation: −0.0148PSA + 0.152CLog*P* + 0.139; *C*log*P* values were estimated with ChemDraw Ultra version 12.0.; (b) Clark, D. E. *J. Pharm. Sci.* **1999**, *88*, 815.
13. The theoretical solubility was calculated using Discovery Studio (DS) 2.55 software. (Accerlys, San Diego, CA, USA).
14. During the preparation of this manuscript, compounds **4a** and **4b** were reported as a synthetic intermediate of the proposed structure of hypoestestatin 1. See Su, B.; Cai, C.; Wang, Q. *J. Org. Chem.* **2012**, *77*, 7981.
15. Kim, S.; Lee, J.; Lee, T.; Park, H.-g.; Kim, D. *Org. Lett.* **2003**, *5*, 2703.
16. For previous alkylation of *N*-Boc-proline methyl ester, see Baran, P. S.; Hafensteiner, B. D.; Ambhaikar, N. B.; Guerrero, C. A.; Gallagher, J. D. *J. Am. Chem. Soc.* **2006**, *128*, 8678.
17. (a) Lee, S. K.; Cui, B.; Mehta, R. R.; Kinghorn, A. D.; Pezzuto, J. M. *Chem. Biol. Interact.* **1998**, *115*, 215; (b) Lee, S. K.; Nam, K. A.; Hoe, Y. H.; Min, H.-Y.; Kim, E.-Y.; Ko, H.; Song, S.; Lee, T.; Kim, S. *Arch. Pharm. Res.* **2003**, *26*, 253; (c) Song, S. H.; Min, H. Y.; Lee, S. K. *Biomol. Ther.* **2010**, *18*, 402.
18. Avdeef, A.; Testa, B. *Cell. Mol. Life Sci.* **2002**, *59*, 1681.
19. Seebach, D.; Boes, M.; Naef, R.; Schweizer, W. B. *J. Am. Chem. Soc.* **1983**, *105*, 5390.
20. Wang, H.; Germanas, J. P. *Synlett* **1999**, 33.
21. Jemal, A.; Siegel, R.; Xu, J.; Ward, E. *CA Cancer J. Clin.* **2010**, *60*, 277.
22. Hong, J.-Y.; Chung, H.-J.; Lee, H.-J.; Park, H.-J.; Lee, S. K. *J. Nat. Prod.* **2011**, *74*, 2102.
23. (a) Hay, N.; Sonenberg, N. *Genes Dev.* **2004**, *18*, 1926; (b) Bjornsti, M. A.; Houghton, P. J. *Cancer Cell* **2004**, *5*, 519–523.
24. Giles, R. H.; van Es, J. H.; Clevers, H. *Biochim. Biophys. Acta* **2003**, *1653*, 1.
25. Kang, Y.-J.; Park, H. J.; Chung, H.-J.; Min, H.-Y.; Park, E. J.; Lee, M. A.; Shin, Y.; Lee, S. K. Mol. Pharmacol. [Online early access]. http://dx.doi.org/10.1124/mol.112.078535. Published Online: May 1, 2012.
26. (a) Burns, B. S.; Edin, M. L.; Lester, G. E.; Tuttle, H. G.; Wall, M. E.; Wani, M. C.; Bos, G. D. *Clin. Orthop. Relat. Res.* **2001**, *383*, 259; (b) Reinecke, P.; Schmitz, M.; Schneider, E. M.; Gabbert, H. E.; Gerharz, C. D. *Cancer Invest.* **2000**, *18*, 614.
27. Kim, E.-H.; Min, H.-Y.; Chung, H.-J.; Song, J.; Park, H.-J.; Kim, S.; Lee, S. K. *Food Chem. Toxicol.* **2012**, *50*, 1060.
28. Frampton, J. E.; Easthope, S. E. *Drugs* **2004**, *64*, 2475.
29. (a) Kitazaki, T.; Oka, M.; Nakamura, Y.; Tsurutani, J.; Doi, S.; Yasunaga, M.; Takemura, M.; Yabuuchi, H.; Soda, H.; Kohno, S. *Lung Cancer* **2005**, *49*, 337; (b) Leggas, M.; Panetta, J. C.; Zhuang, Y.; Schuetz, J. D.; Johnston, B.; Bai, F.; Sorrentino, B.; Zhou, S.; Houghton, P. J.; Stewart, C. F. *Cancer Res.* **2006**, *66*, 4802.
30. Ludescher, C.; Thaler, J.; Drach, D.; Drach, J.; Spitaler, M.; Gattringer, C.; Huber, H.; Hofmann, J. *Br. J. Haematol.* **1992**, *82*, 161.
31. Chou, T. C. *Pharmacol. Rev.* **2006**, *58*, 621.